Anisotropy of photofragment recoil as a function of dissociation lifetime, excitation frequency, rotational level, and rotational constant

Hahkjoon Kim, Kristin S. Dooley, and Simon W. North
Department of Chemistry, Texas A&M University, P.O. Box 30012, College Station, Texas 77842

Gregory E. Hall
Chemistry Department, Brookhaven National Laboratory, Upton, New York 11973-5000

P. L. Houston[a)]
Department of Chemistry and Chemical Biology, Baker Laboratory, Cornell University, Ithaca, New York 14853

(Received 25 April 2006; accepted 25 May 2006; published online 4 October 2006)

Quantum mechanical calculations of photofragment angular distributions have been performed as a function of the frequency of excitation, the lifetime of the dissociative state, the rotational level, and the rotational constant. In the limit of high J values and white, incoherent excitation, the general results are found to agree exactly with both those of Mukamel and Jortner [J. Chem. Phys. **61**, 5348 (1974)] and those of Jonah [J. Chem. Phys. **55**, 1915 (1971)]. Example calculations describe how the anisotropy is dependent on the degree of broadening, the rotational constant, the initial rotational level, and the frequency of excitation. Applications are also made to interpret experimental results on the photodissociation of ClO via the 11-0, 10-0, and 6-0 bands of the $A\,^2\Pi_{3/2}-X\,^2\Pi_{3/2}$ transition and on the photodissociation of O_2 via the 0-0 band of the $E\,^3\Sigma_u^- - X\,^3\Sigma_g^-$ transition. © *2006 American Institute of Physics*. [DOI: 10.1063/1.2216708]

I. INTRODUCTION

The use of photofragment angular distributions to provide insight into excited state symmetry, lifetimes, and dynamics is well documented.[1–9] In diatomic molecules the photofragment angular distributions arising from one-photon dissociation using linearly polarized light can be expressed as[10,11]

$$I(\theta) = \frac{1}{4\pi}(1 + \beta P_2(\cos\theta)), \tag{1}$$

where β is +2 for a purely parallel transition ($\Delta\Omega=0$) and −1 for a purely perpendicular transition ($\Delta\Omega=\pm1$), $P_2(\cos\theta)$ is the second Legendre polynomial, and θ is the angle between the fragment recoil direction and the polarization direction. The normalization factor $1/4\pi$ corresponds to unit probability for the integral of $I(\theta)$ over all solid angles. A value of β intermediate between the extremes of 2 and −1 can have several origins: a mixed transition, depolarization due to an excited state lifetime comparable to the rotational period, or a breakdown of the axial recoil approximation. In polyatomic molecules, reduction in β from its limiting values will also occur when the recoil axis is neither parallel or perpendicular to the transition dipole moment. If the recoil direction is at an angle χ with respect to the transition moment, then the limiting form of β can be calculated as $\beta=2P_2(\cos\chi)$.

There is ample previous work on how and why the anisotropy of photofragment recoil will be reduced from the limiting values. The breakdown of the axial recoil approximation has been considered recently by Demyanenko *et al.*[12] and by Wrede *et al.*[13] Here we concentrate on the reduction due to the effect of the lifetime of the excited state prior to dissociation. This topic has been addressed in a semiclassical model by Jonah,[14] who calculated for a parallel transition that

$$I(\theta) = \frac{\cos^2(\theta)(\tau\omega + 1/\tau\omega) + \tau\omega}{4\tau\omega + 1/\tau\omega}, \tag{2}$$

where τ is the lifetime of the molecule and ω is its classical angular frequency. Note that when $\tau\omega\to0$, $I(\theta)$ is given by a $\cos^2(\theta)$ distribution and β achieves its limiting value of 2, but as the lifetime gets long compared to the reciprocal of the rotational frequency, β is reduced from this limiting value, ultimately by a factor of 4. As satisfyingly simple as are this expression and the corresponding one for a perpendicular transition, they leave open several questions. How will β behave as a function of frequency; i.e., how does it vary across the absorption band? How will it depend on the specific value of J?

Several studies have addressed these questions for the $\tau\omega\to\infty$ limit, i.e., when the absorption lines are sharp and dissociation is slow relative to rotation. For example, Zare demonstrated how to calculate the alignment of molecules by optical absorption, which is directly related to the dissociation anisotropy for long-lived states.[15] More recently, Cosofret *et al.* showed how to perform the calculation for both one- and two-photon excitations using the example of photodissociation of NO.[16] Dixon has recently tabulated β for a variety of multiphoton excitation schemes to dissociative states that live long enough to have sharp lines.[17] However, while these papers do predict β at specified frequencies, they do not address how β changes when the lifetime of

[a)]Electronic mail: plh2@cornell.edu

the dissociation state becomes comparable to or shorter than the rotational period and, thus, they do not address frequencies nonresonant with individual rotation levels.

Mukamel and Jortner did address these questions in 1974.[18] We briefly outline their approach here to put our own into context. The cross section for dissociation from a specified starting state $|g\upsilon JM,\mathbf{k}\rangle$ is given by

$$\sigma_{JM}(\theta,E)=\frac{(2\pi)^2}{\hbar c}\langle\mathbf{K},\upsilon ac|T(E)|g\upsilon JM,\mathbf{k}^2\rho. \tag{3}$$

Here, g is the lower electronic state; υ, its vibrational level; J,M is the rotational state; $\mathbf{k}$ is the photon wave vector, from which linear polarization direction the angle θ is measured; $\langle\mathbf{K},\upsilon ac|$ represents the dissociative state, described by an outgoing plane wave following absorption of the photon; $T(E)$ represents the Hamiltonian; and ρ corresponds to the density of states in the dissociative continuum. Under reasonable assumptions that the various levels decay independently, Mukamel and Jortner find that

$$\langle\mathbf{K},\upsilon ac|T(E)|g\upsilon JM,\mathbf{k}\rangle=\sum_{J'M'}\frac{\langle\mathbf{K}\upsilon ac|H_V|s\upsilon'J'M'\rangle\langle s\upsilon'J'M'|H_{\mathrm{int}}|g\upsilon JM,\mathbf{k}\rangle}{E-E_{J'}+i(\Gamma_{J'}/2)}, \tag{4}$$

where H_V is the part of the Hamiltonian that couples the excited state to the dissociative continuum, H_{int} is the part of the Hamiltonian giving rise to the optical excitation, $\Gamma_{J'}$ is related to the lifetime of the upper level, $\Gamma_{J'}=1/(\pi\tau)$, and the summation is over the various excitation branches, typically P, Q, and R. Their paper then proceeds to evaluate the two matrix elements on the right-hand side (rhs) of (4) in detailed fashion. An intermediate result, of use to us later, is that

$$\sigma_{JM}(\theta,E)=\frac{(2\pi)^2}{\hbar c}(2J+1)\rho\times\sum_{J',J''=J,J\pm1}\frac{R_{J'}R^*_{J''}A_{J'}A_{J''}D^{J'}_{M\Lambda}(\varphi,\theta,0)D^{J''*}_{M\Lambda}(\varphi,\theta,0)}{(E-E_{J'}+i(\Gamma_{J'}/2))(E-E_{J''}-i(\Gamma_{J''}/2))}. \tag{5}$$

Here, R_J involves integrals over the radial part of the wave function, and it is assumed that these do not vary strongly with E over the excitation range. The functions A are the one-photon excitation functions, in this case for linear polarization, while D are rotation matrices. Note that the result in (5) must be summed over all initial JM states that through their broadened lines contribute to excitation at the energy E. Of course, the initial J,M states must be weighted by their populations; for a thermal distribution the weight is simply $\exp[-E(J,M)/kT]/Q_{\mathrm{rot}}$, where $E(J,M)$ gives the energy for this initial state and Q_{rot} is the rotational partition function.

The approach taken here and in Ref. 16 is, essentially, to jump directly to the equivalent of (5). As have both Jonah and Mukamel and Jortner, we assume the axial recoil limit. We write the angular and frequency dependent dissociation probability as

$$\begin{aligned}I(\theta,\nu)=C\sum_{J,M}\mathrm{Pop}(J,M)|&L(\nu,J-1)A(J,M,\Omega_i,\Omega_f,J-1)\\&\times N(J-1)d^{J-1}_{M,\Omega_f}(\theta)+L(\nu,J)A(J,M,\Omega_i,\Omega_f,J)\\&\times N(J)d^{J}_{M,\Omega_f}(\theta)+L(\nu,J+1)A(J,M,\Omega_i,\Omega_f,J+1)\\&\times N(J+1)d^{J+1}_{M,\Omega_f}(\theta)|^2.\end{aligned} \tag{6}$$

In this equation C is a constant; $\mathrm{Pop}(J,M)$ is the population of the initial state, given by $\exp[-E(J)/kT]/Q_{\mathrm{rot}}$, independent of M for an isotropic thermal sample, although polarized or nonthermal distributions are easily represented by other forms of $\mathrm{Pop}(J,M)$; $A(\ldots)$ is a function giving the absorption amplitude for a particular transition; $N(J')=[(2J'+1)/2]^{1/2}$ is a normalization factor (see below); $d^J_{M\Omega}(\theta)$ is a rotation matrix element; and $L(\nu,J')$ is a Lorentzian broadening amplitude given by

$$L(\nu,J')=\frac{(\Delta\nu/2\pi)^{1/2}}{\nu-\nu_{J,J'}+i(\Delta\nu/2)}. \tag{7}$$

Here, $\nu_{J,J'}$ is the center frequency for the particular P, Q, or R transition. The function $L(\nu,J')$ must be complex (rather than, for example, the real square root of the Lorentzian probability) in order to have the correct magnitudes and phases for the off-diagonal products in (6).[19]

A justification for (6) and a route for application to more complicated cases is given as follows. Dissociation from an initial J,M state to produce products at an angle θ is the analog of an experiment where light passes through three slits and strikes a screen. The P, Q, and R excitations correspond to the paths through the three slits and θ corresponds to the final position on the screen. As in the classic interference experiment, the probability amplitudes for the three paths must be added before determining the final probability by squaring (more correctly, by multiplying by the complex conjugate). However, in the dissociation experiment, it is as if the slits have slightly different widths, since the probability amplitude depends not only on the P, Q, or R path through the slightly different values of the function $A(\ldots)$ but also on how far the frequency ν is from the resonance for each of these lines. For each path, the probability depends on the broadening amplitude, on the optical excitation probability amplitude, and on a rotation matrix element.

The optical excitation probability amplitude $A(\ldots)$ is simply an M-state resolved version of the Hönl-London factor; that is, the sum over M of squares of the function $A(\ldots)$ gives the Hönl-London factor. Values of $A(\ldots)$, for both the linear polarization used here and for circular polarization, are tabulated, for example, by Bray and Hochstrasser[20] and easily programed. The rotation matrix element can be interpreted as follows, following the physical interpretation given on p. 92 of Ref. 21: The rotation matrix element $d^J_{M,\Omega_f}(\theta)$ is the probability amplitude that a rotation vector making a projection of M onto one axis will make a projection Ω_f onto another axis rotated from the first by an angle θ. Alternatively put, it is the probability amplitude that, if J makes a projection M onto one axis and Ω_f onto another axis, the two axes will be rotated from one another by an angle θ. In the

case at hand, for example, in the Q branch, the rotation matrix element gives the probability amplitude that if J makes a projection M onto the Z axis (defined as the axis of linear polarization) and a projection Ω_f onto the internuclear axis, the internuclear axis will be at an angle of θ relative to the Z axis. In the axial recoil limit, where the products recoil along the internuclear axis, the distribution of θ thus gives the distribution of products. We conclude that for this description, which is Hund's case (a) coupling (see, for example, the diagram on p. 298 of Ref. 21), the product $d^J_{M,\Omega_f}(\theta)d^{J^*}_{M,\Omega_f}(\theta)$ is simply the angular distribution for the products produced from excited states J, M, and Ω_f in the axial recoil limit.

In summary, for each of the three paths there is an amplitude given by the product of a broadening amplitude, an optical excitation amplitude, and a probability amplitude for dissociation with the internuclear axis at an angle θ with respect to the Z axis. The probability amplitudes are then summed, the sum is multiplied by its complex conjugate to give the probability, and the probabilities are summed over all relevant initial states weighted by their populations. The factor $N(J')=[(2J'+1)/2]^{1/2}$ is a normalization constant for the rotation matrix elements: $(2J'+1)/2\int d^{J'}_{M',N'}(\theta)d^J_{M,N}(\theta)\times\sin\theta d\theta=\delta_{J,J'}\delta_{M,M'}\delta_{N,N'}$, as described in Eq. 3.113 of Ref. 21.

The remainder of this paper is divided as follows. In Sec. II we show that the results of the Jonas formula, the Mukamel and Jortner formulation, and our own are in agreement for the high-J limit and for incoherent, white light excitation. We then apply Eqs. (6) and (7) to cases of isolated P, Q, and R triplets to develop intuition about how β varies as a function of frequency, broadening parameter, and rotational level. In Sec. III we briefly describe experiments at Texas A&M on ClO and at Cornell on O_2. Section IV provides the results of these experiments and presents calculations that help to understand the variation of β with excitation frequency. They also provide a user guide as to how to perform such calculations, both in the more straightforward case such as ClO, where Eqs. (6) and (7) are sufficient, and in the more complicated case such as O_2, where these equations need to be extended to cover, for example, Fano line shapes, more excitation pathways, and behavior intermediate to Hund's cases (a) and (b). Section V provides directions for further extension of this approach as well as concluding remarks. An Appendix provides a formula for extending this approach to more complicated systems.

II. CALCULATED EXAMPLES

We begin this section by showing that Eqs. (1), (5), and (6) all lead to the same prediction for the reduction in β from its limiting values as the lifetime of the excited state increases. Mukamel and Jortner have shown [their Eqs. (4)–(10)], in the limit of broadband incoherent excitation (that is, integration over E) and for a $^1\Sigma-{}^1\Sigma$ transition, that (5) leads to[18]

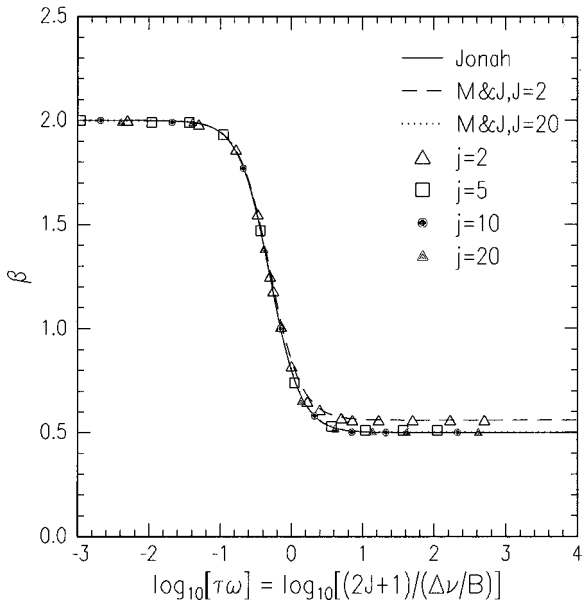

FIG. 1. Comparison of β vs $\log_{10}(\tau\omega)$ for equations of Jonah (Ref. 14) (solid line), Mukamel and Jortner (Ref. 18) (dashed and dotted lines), and this work (individual points) for a variety of values of J.

$$I(\theta)=C_1\left[\cos^2(\theta)-2\frac{J(J+1)}{(2J+1)^2}\frac{\zeta_J^2}{1+\zeta_J^2}P_2(\cos\theta)\right], \tag{8}$$

where $C_1=[(2\pi)^2/\hbar][2\pi/\Gamma]|R_J|^2$ and $\zeta=2B(2J+1)/\Gamma_J$ with B as the rotational constant. To compare (2) and (8) requires a consistent normalization, which can be obtained by replacing C_1 in (8) by $3/(4\pi)$ and by multiplying the rhs of (2) by $3/(4\pi)$. Normalizing (2) and (8) as described and then equating each to (1) produces, in the first case,

$$\beta=2\frac{(1+(\tau\omega)^2)}{(1+4(\tau\omega)^2)}, \tag{9}$$

and in the second,

$$\beta=2\left(1-3\frac{J(J+1)}{(2J+1)^2}\frac{\zeta_J^2}{1+\zeta_J^2}\right). \tag{10}$$

Equating (9) and (10) leads to an equation whose solution, in the high-J limit, gives the correspondence between Jonah's $\tau\omega$ and Γ/B, namely, $\zeta=2\tau\omega$ or $(2J+1)/(\Gamma/B)=\tau\omega$.[22] Note that $\Delta\nu$ in (7) is identical to $\Gamma_{J'}$ in (4).

With this correspondence it is now possible to compare the results of the three approaches. Figure 1 shows that for $J=20$, Eqs. (9) and (10) predict exactly the same curves (the dotted curve cannot be seen because it falls exactly on the solid one). The points calculated from Eq. (6) also lie on these curves. Similar results are obtained for $J=5$ and $J=10$. However, for $J=2$, where the high-J limit is not achieved, the calculations of (6) and (10) are in agreement and are slightly different from those calculated from the Jonah equation, (9). All three approaches correctly predict the decrease in β with increasing $\tau\omega$ for white light excitation in the high-J limit. Note, however, that the implicit J dependence of β for a particular predissociation lifetime in Jonah's classical result (2) does not give correct predictions

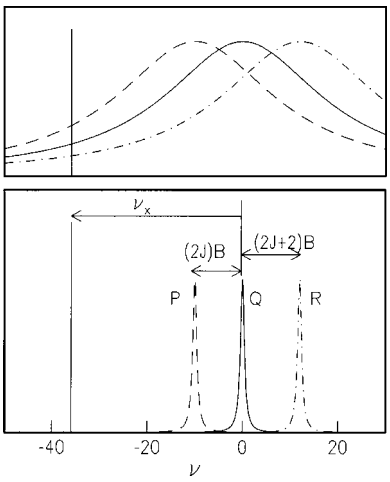

FIG. 2. Excitation of a *P*, *Q*, and *R* triplet under cases where the broadening is much larger than the spacing (top) or much smaller (bottom).

for individually selected rotational lines, but only for the uncommon case of broadband excitation from an isotropic sample of a single initial *J* state.

The exact agreement between the approach of (6) and that of Mukamel and Jortner is not surprising, once one examines the correspondence between (6) and (5). In the latter equation, a normal approximation is to assume that the R_J functions are not strongly dependent on *J*, so that they can be pulled out of the sum and incorporated into an overall constant. Multiplication of the *D* rotation matrices produces cancellation of the factors involving the azimuthal variable to give the reduction $d^{J'}_{M,\Lambda}(\theta)d^{J''*}_{M\Lambda}(\theta)$. Mukamel and Jortner considered only singlet states, where $\Omega=\Lambda$. For parallel polarization $M'=M$, so summation over this factor is not needed. The factors A_J functions of (5) are identical to the $A(\ldots)$ functions of (6). Finally, the summation in (5) over $J',J''=J,J\pm1$ produces nine terms. These nine terms correspond to the nine terms produced in (6) when the three-term sum in that equation is multiplied by its complex conjugate. The only differences involve equivalent ways of writing the normalization and broadening terms and the omission in (5) of the Boltzmann factor, which is included elsewhere in the Mukamel and Jortner approach. Thus, under reasonable assumptions about R_J, the approaches represented by (5) and (6) are equivalent.

We now use Eq. (6) to develop some intuition about how β should vary with ν for simple cases, since this variation is not treated by Jonah. Figure 2 illustrates two extreme cases. In the bottom panel, a single frequency located ν_x from the *Q* line will produce nearly zero absorption unless ν_x is nearly resonant with one of the lines; the broadening of the lines is too small to provide much amplitude at other frequencies. In the top panel, the broadening is much larger, so all three lines are excited together with amplitudes that differ but are of similar magnitude.

Figures 3–5 show how β and the absorption due to a single *P*, *Q*, and *R* triplet vary with ν for a parallel transition and for differing values of $\Delta\nu/B$. The spectrum is generated from (6) simply by integrating the angular distribution over $\sin\theta d\theta$. In each panel, the dashed line gives β, as read from the right-hand ordinate, while the solid line gives the spectrum, in arbitrary units, as read from the left-hand ordinate. The panels show the results for increasing *J* from bottom to top. In Fig. 3, the lines are very sharp compared to the spacing between them, so as the frequency is scanned each line makes a nearly "separate" contribution. By "separate," we mean that although all lines experience the radiation, the weighting factor in (6) for the one on resonance is so much larger than that for the other two that the other two make little contribution. Note that the contribution from the *Q* line is small for this parallel transition ($\Omega''=1$ to $\Omega'=1$), but that the value of β at the wavelength corresponding to the *Q* line is negative. Of course, since the intensity is small, measurement of β at this frequency would be difficult at high *J*.

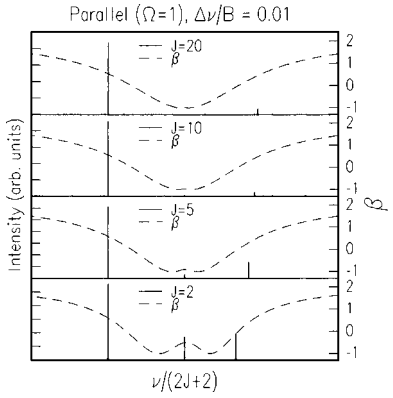

FIG. 3. β and spectrum as a function of *J* for $\Delta\nu/B=0.01$ and a parallel transition.

The predictions for β at the frequencies in resonance with the *P*, *Q*, and *R* lines are in agreement with the sharp-line calculations of Zare.[15] For an $\Omega=0$ to $\Omega=0$ transition (not shown in the figures), β at, for example, the *R*(2), *R*(5), and *R*(15) lines is 0.80, 0.64, and 0.55, respectively, while for the *P*(2), *P*(5), and *P*(15) lines it is 0.20, 0.36, and 0.45, respectively. These are equal to the values that are calculated from Eqs. (9) and (10) of Ref. 15. In the limit of high *J*, these values approach 0.5. Similar behavior at high *J* can be seen in Fig. 3.

In Fig. 4, the broadening is comparable to the spacing between lines at low *J*, and the curves for β as a function of ν are not much changed. Again, there is significant intensity

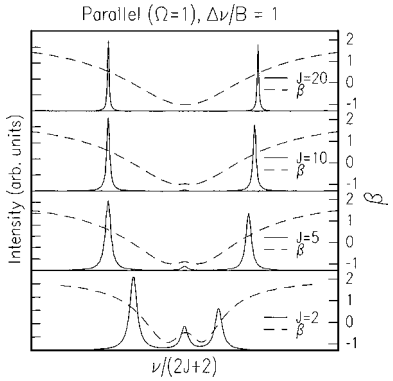

FIG. 4. β and spectrum as a function of *J* for $\Delta\nu/B=1$ and a parallel transition.

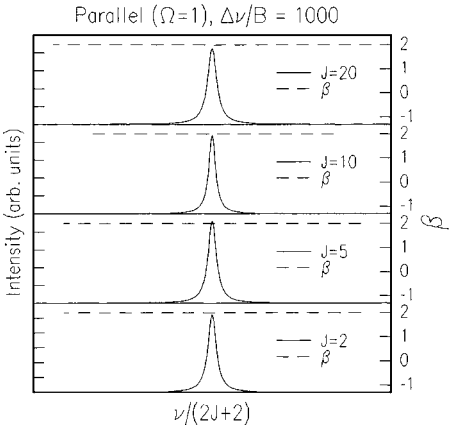

FIG. 5. β and spectrum as a function of J for $\Delta\nu/B=1000$ and a parallel transition.

only near the line centers, but over a somewhat broader range. Siebbeles and co-workers,[23,24] in their experiments on triplet hydrogen, scanned the excitation laser frequency over two resonances $[Q(1)$ and $R(1)]$ and observed all possible values between -1 and 2 of the photofragment anisotropy parameter β. Their results and calculations show the same behavior as depicted in the bottom trace of Fig. 4.

In Fig. 5, the broadening is much larger than the spacing between the individual lines, and the envelope of the absorption shows a Lorentzian profile (the abscissa for this figure covers considerably more spectral range than that for Figs. 3 and 4). The P, Q, and R contributions to the amplitude are now similar at nearly all frequencies, and β is uniformly equal to its limiting value of 2 across the spectrum. Note that this value is substantially larger than the value for any separate line when, as in Fig. 3, the lines are sharp. The limiting values of β are most readily achieved when the amplitudes of the P, Q, and R contributions in the sum of Eq. (6) are nearly equal. Indeed, it is the coherence of the excitation that leads to the limiting value.

Similar calculations have been performed for a perpendicular transition, with similar results, except of course that the limiting value for β is -1.

Since β is so sensitive to the coherent nature of the excitation, one might wonder whether a spectral simulation would need to be performed using (6) or whether it could be performed in the usual way of treating the contribution from each line separately. Fortunately, it is easy to show that the latter case is obtained. When the sum in (6) is multiplied by its complex conjugate, there will be diagonal terms involving, for example, the term for the P line multiplied with its complex conjugate, and off-diagonal terms involving products of, for example, the P term and the complex conjugate of the Q term. At a given angle θ, these off-diagonal terms are important for determining scattering, and they thus affect β. On the other hand, when one integrates over $\sin\theta d\theta$, the cross terms vanish due to the aforementioned orthogonality (Eq. 3.113 in Ref. 21) of the $d^J_{M,\Omega_f}(\theta)$ matrix elements. Thus, if one were to want only the spectral simulation and not $\beta(\nu)$, one could reasonably perform the simulation line by line. However, if $\beta(\nu)$ is desired, one must be careful to consider together and coherently all paths from each initial state to a final scattering angle θ, as in (6).

III. EXPERIMENT

A. Photodissociation of ClO

The Texas A&M University velocity-map ion-imaging apparatus used in the ClO experiments has been described in detail elsewhere.[25,26] Briefly, a pulsed, collimated, ClO molecular beam was intersected at 90° by two copropagating linearly polarized laser beams from the frequency doubled output of two Nd:YAG (yttrium aluminum garnet) pumped dye lasers. Both fundamental wavelengths were calibrated using a Ne-filled hollow cathode lamp. The photolysis beam was provided by a Nd:YAG (Spectra Physics GCR-150-10) pumped dye laser (Spectra Physics PDL-1) after frequency doubling. Four Pellin-Broca prisms were used to maintain overlap of the photolysis and probe laser beams during the photofragment excitation (PHOFEX) scans. Typical photolysis and probe pulse energies were 20 and 30 μJ, respectively. The $Cl(^2P_{3/2})$ atoms were probed using 2+1 REMPI (resonantly enhanced multiphoton ionization) transition at 235.336 nm $(4p^2D_{3/2}\leftarrow 3p^2P_{3/2})$ (Ref. 27) and the $O(^3P_0)$ atoms were probed using the 2+1 REMPI transition near 226 nm $(3p^3P_{2,1,0}\leftarrow 2p^3P_{2,1,0})$.[28] The resulting chlorine and oxygen cations were accelerated by velocity mapping ion optics[29] prior to entering a 50 cm long field-free flight tube along the axis defined by the molecular beam. The ions were projected on a position-sensitive detector consisting of a dual microchannel plate-phosphor assembly. Images were acquired using a charge-coupled device (CCD) camera and a frame grabber controlled by a commercial software (CODA32) which involved centroiding and event counting.[30] The final $O(^3P_0)$ images were obtained by repeatedly scanning Doppler profiles over the REMPI transitions to achieve homogeneous detection efficiency. The three dimensional velocity distributions were reconstructed from the two-dimensional projections using the basis set expansion (BASEX) algorithm developed by Drinbinski *et al.*[31] The ClO molecular beam was generated using the flash pyrolysis of a Cl_2O/He mixture as described previously.[25] Simulations of the PHOFEX spectra (*vide infra*) indicates that the radicals are characterized by $T_{\rm rot}\leqslant 100\pm 20$ K with negligible vibrational and electronic excitations.

B. Photodissociation of O_2

The experimental procedure and primary data have already been presented in detail elsewhere,[32] so they will be summarized only briefly here. A molecular beam of oxygen entered an ion imaging apparatus and was crossed at right angles with copropagating light of 120.4 and 130.2 nm. Each laser wavelength was generated by four-wave difference frequency generation in krypton using the same 212.55 nm light for the two-photon transition in krypton and using two visible wavelengths, 729 and 578 nm, to obtain 120.4 and 130.2 nm, respectively. The former wavelength excited O_2 on the 0-0 band of the $E\,^3\Sigma_u^- - X\,^3\Sigma_g^-$ transition, while the latter wavelength excited $O(^3P)$ products in the first step of a

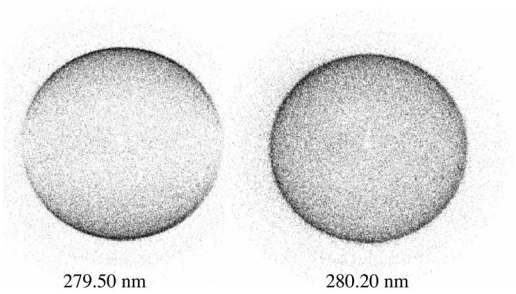

FIG. 6. Raw $O(^3P_0)$ ion images arising from ClO photodissociation in the 10-0 band of the $A\ ^2\Pi_{3/2}$ state.

$1+1'$ ionization scheme, where the second photon was residual light from the 212.55 source. $O(^1D)$ was also probed by 2+1 REMPI using light at 203.7 nm. Photofragment yield spectra were generated by scanning the wavelength of the source centered at 120.4 nm while recording the signal intensity of the probed $O(^1D_2)$ or $O(^3P_2)$. Angular and speed distributions were obtained for each of $O(^1D_2)$, $O(^3P_2)$, and $O(^3P_0)$ at five specific dissociation wavelengths. The angular distributions were analyzed and found to indicate significant alignment of the $O(^1D)$ and $O(^3P_2)$ fragments, with production of mostly $m_J=0$. The values of β at the five wavelengths were reasonably consistent across the pairs of recoiling fragments, although there was substantial error from the experiment and from the fitting procedure. As expected, the angular distributions indicated a basically parallel transition, with values ranging between $\beta=0.74$ and 1.53. The results are summarized in Table II of Ref. 32 and will be presented graphically in Sec. IV.

IV. RESULTS AND DISCUSSION

A. Photodissociation of ClO

The predissociation of the ClO $A\ ^2\Pi_\Omega$ state represents an ideal system to test the modeling of fragment spatial anisotropy. Excitation to the $A\ ^2\Pi_{3/2}$ state involves a parallel ($\Delta\Omega=0$) corresponding to an intrinsic anisotropy parameter of $\beta=2.0$ in the limit of prompt recoil. There have been numerous spectroscopic studies of the $A\ ^2\Pi_\Omega$ state and the spectroscopic constants are well known.[33–37] The $A\ ^2\Pi_{3/2}$ state, which correlates to $O(^1D)$, is bound but is predissociated by a number of repulsive states which correlate to $O(^3P)$. The individual vibronic bands of the $A\ ^2\Pi_{3/2}$ state exhibit partially resolved rotational structure with the resolution of each band dependent on the predissociation lifetimes, which vary from 0.5 to 10 ps. The lifetimes do not depend on J, suggesting that predissociation is due to spin-orbit coupling and not induced by molecular rotation. Our previous investigations of ClO produced beams with rotational temperatures near 100 K, a temperature which provides access to a wide range of rotational states, $J>20$, with reasonable signal-to-noise ratio. These factors permit coarse "tuning" of the number of overlapping transitions to explore the limits of the current model. In addition, since the $O(^3P_0)$ fragment has no angular momentum, the ion images are sensitive only to the spatial anisotropy, avoiding complications involving atomic alignment.

In this work we have measured spatial anisotropy parameters for the $O(^3P_0)$ fragments arising from the predissociation of the ClO $A\ ^2\Pi_{3/2}$ state throughout the 10-0 and 6-0 vibronic bands and in sections of the 11-0 band. These bands were selected primarily due to their different lifetimes, 2.5, 1.0, and 0.5 ps for the 11-0, 10-0, and 6-0 bands, respectively. Figure 6 shows raw $O(^3P_0)$ images (upper panel) arising from ClO photodissociation at 279.50 and 280.20 nm corresponding to excitation at the band head and in the tail region on the 10-0 band, respectively. Photodissociation of the 6-0, 10-0, and 11-0 bands results in the production of only $Cl(^2P_{3/2})$ fragments in coincidence with $O(^3P_0)$ fragments, and therefore the images consist of a single ring. The difference in the spatial anisotropy arising from photodissociation at the two wavelengths is clear from inspection of the raw images. Anisotropy parameters derived from the images for both vibronic bands are shown as the upper data points in Figs. 7 and 8.

In order to provide wavelength calibration and to determine the rotational temperature, we collected PHOFEX spectra for each band investigated. PHOFEX spectra were obtained through analysis of $Cl(^2P_{3/2})$ ion images acquired across each band rather than by collecting total ion signal associated with either $O(^3P_0)$ or $Cl(^2P_{3/2})$ products. Since the PHOFEX is a relative signal, a small feature in the ion images due to Cl_2 photodissociation was used as a constant intensity reference to which the strongly wavelength-dependent ClO feature was compared. Such analysis required us to assume that the contribution from Cl_2 photodissociation, due to a broad absorption spectrum in this region, was constant over each run (despite large run-to-run variability in the overall Cl_2 signal). Our experience suggested that this assumption was reasonable. A comparison of the relative intensities of the Cl_2 photodissociation and ClO photodissociation contributions to the speed distributions also provided correction for beam overlap and probe power. We find that the PHOFEX experiments were highly reproducible.

Figure 7 shows the photofragment excitation spectrum of ClO on the 10-0 band of the $A\ ^2\Pi_{3/2}-X\ ^2\Pi_{3/2}$ transition as well as the experimental measurements of β at several wavelengths. Equation (6) was used to calculate the spectral simulation and the variation of β with wavelength.[38] The results are given as solid lines, calculated for $\Delta\nu=4.0\ \mathrm{cm}^{-1}$. The spectral simulation parameters were $B''=0.623\ 45\ \mathrm{cm}^{-1}$, $B'=0.360\ 13\ \mathrm{cm}^{-1}$, $\nu_{00}=35\ 752.74\ \mathrm{cm}^{-1}$, and $T=100$ K. Rotational levels up to $J=49$ were included.

Figure 8 shows a similar photofragment excitation spectrum for ClO on the 6-0 band of the $A\ ^2\Pi_{3/2}-X\ ^2\Pi_{3/2}$ transition. The results are calculated for $\Delta\nu=10.0\ \mathrm{cm}^{-1}$. The spectral simulation parameters were the same for the ground state as in the 10-0 calculation: $B'=0.389\ \mathrm{cm}^{-1}$, $\nu_{00}=34268.43\ \mathrm{cm}^{-1}$, and $T=80$ K. Note that the broadening is higher for the 6-0 band than for the 10-0 band, resulting generally in higher values of β, as might be expected from comparing Figs. 4 and 5.

Encouraged by these results, we attempted to see if one

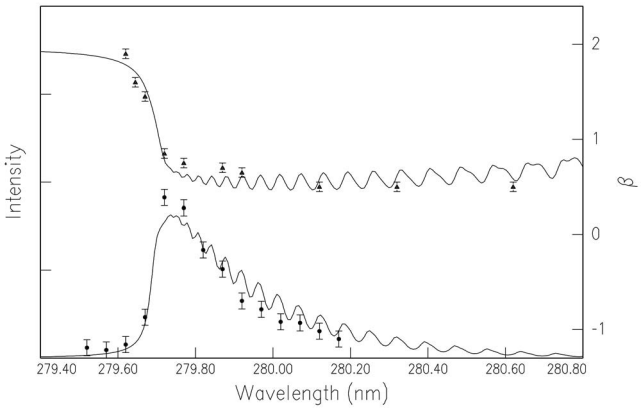

FIG. 7. Experimental data for the 10-0 band of ClO and calculated spectrum and variation in β. The solid triangles give the experimental values of β (right hand ordinate), while the diamonds give the experimental photofragment excitation spectrum. The calculations were done for $\Delta\nu=4.00\ \mathrm{cm}^{-1}$.

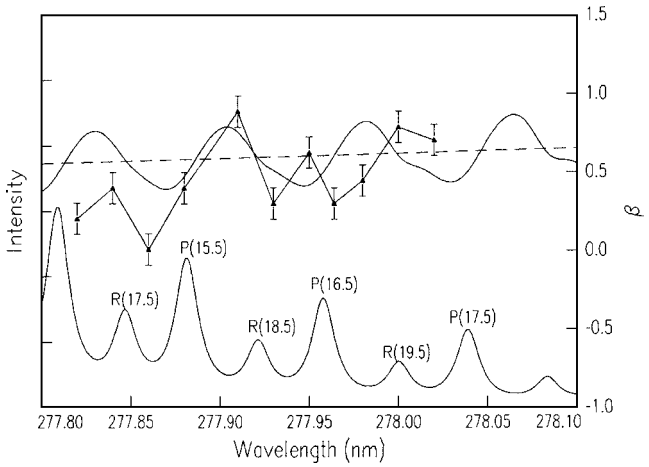

FIG. 9. Experimental data for the ClO 11-0 band (triangles with error bars) and calculated values for the spectrum and the variation of β with wavelength. The dashed line gives the average trend of β in this region.

could observe oscillations in β predicted, for example, in Fig. 7. Figure 9 presents results for the 11-0 band, for which the lifetime broadening is known to be much smaller than in the 6-0 or 10-0 bands. For the 11-0 band, the broadening of 2 cm^{-1} is comparable to the spacing between transitions involving the higher J values, so that it is possible in theory to measure how β changes when the dissociation laser is slightly off resonance versus on resonance. Eleven images were taken at roughly equal spacings between 277.85 and 278.05 nm and analyzed to determine the anisotropy parameter. The results are plotted as points with error bars in the figure, which also shows the prediction of (6) as well as the simulation of the (unmeasured) spectrum. The spectroscopic constants for the ground virbational level were the same as those used above, whereas the rotational constant for $v=11$ was taken to be $B=0.345\ \mathrm{cm}^{-1}$. The value for ν_{00} was 36 068.75 cm^{-1}. The dashed line gives the average trend of β in this region.

Despite the difficulty of the experimental measurements, there are two important points to notice about the data. First, the data show an oscillation of β around the average value predicted by the theory of (6), roughly in phase with theory. Second, the magnitude of the oscillation is in approximate agreement with the prediction of (6).

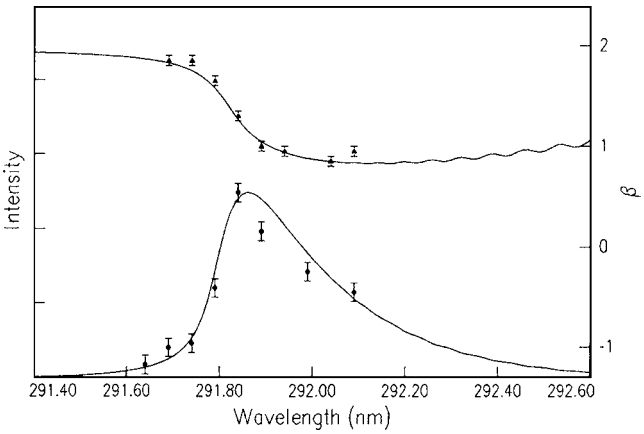

FIG. 8. Experimental data for the 6-0 band of ClO and calculated spectrum and variation in β. The solid triangles give the experimental values of β (right hand ordinate), while the diamonds give the experimental photofragment excitation spectrum. The calculations were done for $\Delta\nu=10.00\ \mathrm{cm}^{-1}$.

It is interesting to note that the oscillations are not in accord with a classical model. A classical model based on (2) might predict an oscillation between β values for the P vs R transitions, due to their different J values and branches, but that is not what is predicted by the quantum model. In the quantum model the value of β in resonance with either P- or R-branch transitions is substantially the same; the oscillation occurs between the resonances. A better understanding of the theory comes from investigating the predicted β variation in correlation with the predicted line positions. In this region of the spectrum, the R branch has turned around from its band head, and the spectrum consists of alternating P- and R-branch transitions, of which four P- and four R-branch transitions fall within the region illustrated. The P-branch transitions have higher amplitude because the adjacent R-branch transitions are from higher J values with lower population. The R-branch transition corresponding to the $P(15.5)$ transition in the figure is at lower wavelength (off this figure). Recall from Fig. 3 that, for a single P,R pair, β is lower between the P- and R-branch transitions and higher outside this range. Thus, we expect β to be lower on the low wavelength side of the P-branch transition (in the direction of the corresponding R) and higher on the high wavelength side, exactly as predicted by (6). It is encouraging that the experiment observes oscillations of approximately the correct magnitude and phase. We conclude that such oscillations should be observable in other systems where the line broadening is comparable to the spacing between rotational lines.

B. Photodissociation of O_2

The photodissociation of O_2 provides some interesting new features compared with the case of ClO. For one thing, the spectroscopy is more complicated because the transition is $E\,^3\Sigma_u^- - X\,^3\Sigma_g^-$. Second, only odd N levels of ground-state O_2 are populated due to the nuclear spin statistics. Third, because the transition is embedded in an optically allowed continuum, Fano line shapes are encountered.[39] Finally, the

transition is an intermediate case between Hund's cases (a) and (b), so the wave function and transition amplitudes must be modified.[40]

The incorporation of Fano line shapes is reasonably straightforward. The factor $L(\nu,J')$ given in (7) should be replaced by $F(\nu,J')=g[q+((\nu-\nu_C)/g)]/[\nu-\nu_C+ig]$, where g is the broadening parameter and q measures the strength of the continuum coupling. In the case of O_2, $q=q_0+q_N(J'(J'+1))^2$ and $g=g_0+g_N(J'(J'+1))$, with $q_N=2.8\times10^{-5}$ and $g_N=0.18$.[41] We have treated q_0 and g_0 as adjustable parameters.

$^3\Sigma$ electronic states intermediate between cases (a) and (b) have been considered by Tatum and Watson.[40] Briefly, the energy levels are given by

$$F_1(J)=BJ(J+1)+(2\lambda-\gamma)-\left(\lambda-B+\frac{1}{2}\gamma\right)-\left[\left(\lambda-B+\frac{1}{2}\gamma\right)^2+4J(J+1)\left(B-\frac{1}{2}\gamma\right)^2\right]^{1/2},$$

$$F_2(J)=BJ(J+1)+(2\lambda-\gamma), \tag{11}$$

$$F_3(J)=BJ(J+1)+(2\lambda-\gamma)-\left(\lambda-B+\frac{1}{2}\gamma\right)+\left[\left(\lambda-B+\frac{1}{2}\gamma\right)^2+4J(J+1)\left(B-\frac{1}{2}\gamma\right)^2\right]^{1/2}.$$

The common term $(2\lambda-\gamma)$ is normally included in the electronic energy. For the 0-0 band of the $E\ ^3\Sigma_u^- - X\ ^3\Sigma_g^-$ transition in O_2, $B''=1.437\,77$, $\lambda''=1.984$, and $\gamma''=0.008\,37$, all in cm^{-1}, while $B'=1.4701$, $\lambda'=-3.3725$, and $\gamma'=0.045$. Note that each rotational state N will be split into three spin-rotation states $J=N+1$, N, and $N-1$ corresponding to the F_1, F_2, and F_3 states, respectively.

The wave functions for the three states are given by

$$|F_1(J)\rangle=c_J|^3\Sigma_0,JM\rangle+2^{1/2}s_J\{|^3\Sigma_1,JM\rangle+|^3\Sigma_{-1},JM\rangle\},$$

$$|F_2(J)\rangle=2^{1/2}\{|^3\Sigma_1,JM\rangle-|^3\Sigma_{-1},JM\rangle\}, \tag{12}$$

$$|F_1(J)\rangle=s_J|^3\Sigma_0,JM\rangle-2^{1/2}c_J\{|^3\Sigma_1,JM\rangle+|^3\Sigma_{-1},JM\rangle\},$$

where

$$c_J=\left[\frac{F_2(J)-F_1(J)}{F_3(J)-F_1(J)}\right]^{1/2},$$

$$s_J=\left[\frac{F_3(J)-F_2(J)}{F_3(J)-F_1(J)}\right]^{1/2}. \tag{13}$$

Note that for every value of N, there will be, in general (except for $N=1$), 14 branches,[40] of which five will have identical values of $J''=N-1$ and $F''=3$, five will have $J''=N+1$ and $F''=1$, and four will have have $J''=N$ and $F''=2$. These several branches starting from a single initial state then replace the P, Q, and R branch terms in (6)—instead of a three slit analog, we have a four or five slit analog. For a transition from F'' to F', the functions that replace $A(\ldots)$ in (6) have modified amplitudes. These can be calculated by evaluating $\langle F'(J)|H_{\rm int}|F'(J)\rangle$ using (12) and the normal definitions for $A(\ldots)$. The matrix element for the transition from $F''=1$ to $F'=3$, for example, is

$$c_{J''}s_{J'}A(J'',M,\Omega''=0,\Omega'=0,J')-\left(\frac{c_{J'}s_{J''}}{2}\right)[A(J'',M,\Omega''=1,\Omega'=1,J')+A(J'',M,\Omega''=-1,\Omega'=-1,J')]. \tag{14}$$

When the squares of these and the other similar terms are summed over M, they provide the modified Hönl-London factors listed for the 14 branches in Table 2 of Tatum and Watson. From the point of view of the Mukamel-Jortner treatment, these modified Hönl-London factors are the squares, summed over M, of the matrix elements $\langle s\omega J'M'|H_{\rm int}|g\omega JM,\mathbf{k}\rangle$ given in (4). The equivalent of the rotational part of the matrix element $\langle\mathbf{K}|H_V|s\omega J'M'\rangle$ in (4) is simply proportional to a function of the form of (12) in which $d^J_{M,\Omega_f}(\theta)$ replaces $|^3\Sigma_{\Omega_f},JM\rangle$. Thus each of the terms in (6) that substitute for the P, Q, and R terms will be of the form of a broadening amplitude, given by $F(\nu,J')$, multiplied with a factor of the form of (14), replacing $A(\ldots)$, multiplied with a factor of the form of (12) with the substitution of the rotation matrix element, as just described. The Appendix provides a concise summary.

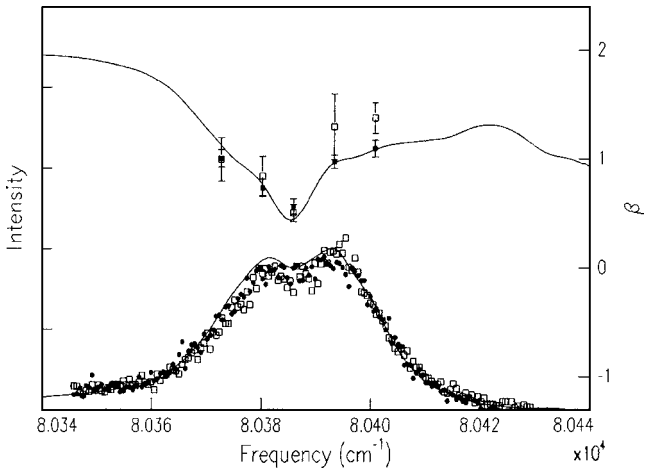

FIG. 10. Experimental results and calculations for the spectrum and variation of β for the 0-0 band of the $E\ ^3\Sigma_u^- - X\ ^3\Sigma_g^-$ band in O_2. The open symbols correspond to measurements of $O(^3P)$, while closed ones correspond to measurements of $O(^1D)$. The solid lines are the results of the calculation.

Calculations were performed using the spectroscopic constants given above with $\nu_{00}=80\,382.8$ cm^{-1}. The results are compared to the measured values of β and the photofragment excitation spectrum in Fig. 10. The parameters that best fit the data are $q_0=-12.0$, $g_0=5.0$ cm^{-1}, and $T=20$ K.

V. CONCLUSION

The good agreement between experimental and calculated values of the yield spectra and the variation of β with ν show that the approach of (6) or, equivalently, of (5) can be useful in interpreting spectroscopic and anisotropy results. An advantage of this approach is that it can be modified relatively easily to cover new situations as they arise.

For example, for two-photon excitation only minor modifications are needed. The principle is the same, in that the sum in (6) must coherently combine all the possible routes from initial states to products at a particular angle. Generally, this will involve the product of $A(\ldots)$ functions going through states of the (virtual) intermediate. This approach has been taken, for example, in a study of the two-photon photodissociation of NO through Rydberg levels in the 265–278 nm region.[16]

If results are desired for different Hund's cases, the wave functions can be modified as done above for O_2, where both electronic states were of mixed character, or as done in the NO study,[16] where different Hund's cases describe the upper and lower electronic states. See also the Appendix.

Extension to polyatomic molecules, either symmetric or asymmetric tops, should be possible by treating the initial state as $|JKM\rangle$ and replacing $A(\ldots)$ with the appropriate linear excitation amplitudes. When the projection of the electronic angular momentum onto the top axis is zero or much smaller than K, the situation is particularly simple. In the case of symmetric tops, the $A(\ldots)$ functions[42] are the same as those listed in Bray and Hochstrasser[20] with K replacing Ω. The rotation matrix element $d^{J'}_{M',K'}(\theta)$ then gives the probability amplitude that the figure axis, where J' makes projection K', will be at an angle θ with respect to Z, where J' makes projection M'. With these substitutions, (6) predicts the angular distribution for the figure axis. If this axis is also the recoil axis, then the distribution gives β; if the recoil axis is rotated from the figure axis by an amount χ, then β will be reduced from the value for the figure axis by a factor $P_2(\cos\chi)$, as can be calculated using the spherical harmonic addition theorem.

Use of circular rather than linear polarization is also straightforward, since Bray and Hochstrasser have given the one-photon versions that correspond to $A(\ldots)$.[20]

Finally, it will be interesting to extend the current approach to excitation by coherent light, whose bandwidth is broad compared to the spectrum.

In summary, we have investigated how β changes as a function of ν and the broadening parameter(s) for situations intermediate between short and long upper state lifetimes relative to the rotational period of the dissociating molecule. A practical method is provided for calculating $\beta(\nu)$, which has the side benefit of additionally generating a simulated spectrum by simply integrating the angular distribution at each wave number over $\sin\theta d\theta$. Despite the long history and importance of the anisotropy parameter, it is surprising that calculations of $\beta(\nu)$ are not routinely performed. The method for doing so was described in 1974,[18] but was somewhat cumbersome. Perhaps the more descriptive treatment given above, in the Appendix, and in the available computer program[43] will encourage better use of this tool.

ACKNOWLEDGMENTS

The work at Texas A&M was supported by the Robert A. Welch Foundation (Grant No. A-1402). The work at Brookhaven National Laboratory was performed under Contract No. DE-AC02-98CH10886 with the U.S. Department of Energy and supported by its Division of Chemical Sciences, Office of Basic Energy. The work at Cornell was supported by the National Science Foundation under Grant No. CHE-0548867. One of the authors (S.W.N.) would like to acknowledge Mike White at Brookhaven National Laboratory for the PDL used in these experiments.

APPENDIX: THE GENERAL CASE

Although Eq. (6) contains the essential physics, individual spectroscopic cases can be more complicated both because of parity considerations and because coupling cases intermediate to cases (a) and (b) are often encountered. Zare has outlined[21] how parity and intermediate behavior can be considered by expressing the wave functions of the initial and dissociative states as linear combinations of case (a) wave functions. Indeed, this is the approach that has been taken by Tatum and Watson.[40] The wave functions for the initial (double prime) and dissociative (single prime) states are expanded as

$$\Psi(J'',M'',P'',F'') = \sum_{\Omega=-\Omega''}^{\Omega''} \alpha''_{\Omega''}\Phi(J'',M'',\Omega''),$$
$$\Psi(J';M',P',F') = \sum_{\Omega=-\Omega'}^{\Omega'} \alpha'_{\Omega'}\Phi(J',M',\Omega'), \tag{A1}$$

where J, M, P, and F are the total rotation, projection, and parity quantum numbers, and F labels the spectroscopic branches based on coupling of nuclear rotation N with electron spin S; and $\Omega=\Sigma+\Lambda$ is the sum of projections in case (a) of the orbital and spin angular momenta onto the internuclear axis. The coefficients of the expansion α_Ω are often simple numbers $(\pm1, \pm1/\sqrt{2}, 0)$, but in cases intermediate between (a) and (b) they can be more complicated functions of J. The formula corresponding to (6) then becomes

$$I(\theta,\nu) = C \sum_{J'',M'',P'',F''} \mathrm{Pop}(J'',M'',F'') \times \left| \sum_{J'=J''-1}^{J''+1} \left\{ \sum_{M',P'F',\Omega'',\Omega'} \alpha''_{\Omega''}\alpha'_{\Omega'} L(\nu,J'',F'',J',F') \times A(J'',M'',\Omega'',\Omega',J') \right\} \times \left\{ N(J') \sum_{\Omega'} \alpha'_{\Omega'} d^{J'}_{M',\Omega'}(\theta) \right\} \right|^2. \tag{A2}$$

Within the absolute value squared term, the first term in braces gives the transition amplitudes, while the second term in braces gives the angular part of the outgoing wave function. The summation over M' can be truncated to $M'=M''$ for linear polarization, while the summation over P' is limited to $P'=-P''$ for electric dipole transitions. A program performing this calculation is available.[43]

[1] R. Bersohn, ACS Symp. Ser. **770**, 19 (2000).
[2] S.-C. Yang and R. Bersohn, J. Chem. Phys. **61**, 4400 (1974).

[3] G. E. Busch and K. E. Wilson, J. Chem. Phys. **56**, 3638 (1972).
[4] R. J. Gordon and G. E. Hall, Adv. Chem. Phys. **96**, 1 (1996).
[5] P. L. Houston, J. Phys. Chem. **91**, 5388 (1987).
[6] G. E. Hall and P. L. Houston, Annu. Rev. Phys. Chem. **40**, 375 (1989).
[7] P. L. Houston, Acc. Chem. Res. **22**, 309 (1989).
[8] M. N. R. Ashfold, N. H. Nahler, A. J. Orr-Ewing, O. P. J. Vieuxmaire, R. L. Toomes, T. N. Kitsopoulos, I. A. Garcia, D. A. Chestakov, S.-M. Wu, and D. H. Parker, Phys. Chem. Chem. Phys. **8**, 26 (2006).
[9] A. J. Orr-Ewing and R. N. Zare, Annu. Rev. Phys. Chem. **45**, 315 (1994).
[10] R. N. Zare, Ph.D. thesis, Harvard University, Cambridge, MA, 1964.
[11] R. N. Zare and D. R. Herschbach, Proc. IEEE **51**, 173 (1963).
[12] A. V. Demyanenko, A. B. Potter, V. Dribinski, and H. Reisler, J. Chem. Phys. **117**, 2568 (2002).
[13] E. Wrede, E. R. Wouters, M. Beckert, R. N. Dixon, and M. N. R. Ashfold, J. Chem. Phys. **116**, 6064 (2002).
[14] C. Jonah, J. Chem. Phys. **55**, 1915 (1971).
[15] R. N. Zare, Ber. Bunsenges. Phys. Chem. **86**, 422 (1982).
[16] B. R. Cosofret, H. M. Lambert, and P. L. Houston, J. Chem. Phys. **117**, 8787 (2002).
[17] R. N. Dixon, J. Chem. Phys. **122**, 1 (2005).
[18] S. Mukamel and J. Jortner, J. Chem. Phys. **61**, 5348 (1974).
[19] In calculations using (6) for situations where the starting distribution of M is isotropic, it can be shown that $I(\theta)$ will vary as $(1/4\pi)\{1+\beta P_2(\cos\theta)\}$. It is then sufficient to calculate the angular distribution at only two angles, for example, $\theta=0$ and $\theta=\pi/2$, from which two values $I(\theta)$ can be used to calculate both β and the amplitude of the absorption.
[20] R. G. Bray and R. M. Hochstrasser, Mol. Phys. **4**, 1199 (1976).
[21] R. N. Zare, *Angular Momentum* (Wiley-Interscience, New York, 1988).
[22] It is interesting to note that this is not the correspondence that one might have expected from $\frac{1}{2}I\omega^2=J(J+1)hcB$ or $\omega^2=J(J+1)2hcB/I$. From the definition of B, we have $hcB=h^2/(8\pi^2 I)$, or $I=h/(8\pi^2 cB)$. Replacing I in the equation for ω^2 gives $\omega^2=J(J+1)16\pi^2c^2B^2$, or $\omega=\mathrm{sqrt}(J(J+1))4\pi cB$. Since $\tau=1/(c\pi\Delta\nu)$, then $\tau\omega=\mathrm{sqrt}(J(J+1))\ (4B/\Delta\nu)$. For high J, we may replace $J(J+1)$ by $J^2+J+(1/4)$ or by $(1/4)(2J+1)^2$. Then we expect that $\tau\omega=4(1/2)(2J+1)/(\Delta\nu/B)=2(2J+1)/(\Gamma/B)$. This is just twice the value given by equating (9) and (10).
[23] M. Glass-Maujean and L. D. A. Siebbeles, Phys. Rev. A **44**, 1577 (1991).
[24] L. D. A. Siebbeles, J. M. Schins, J. Los, and M. Glass-Maujean, Phys. Rev. A **44**, 1584 (1991).
[25] H. Kim, J. Park, T. C. Niday, and S. W. North, J. Chem. Phys. **123**, 174303 (2005).
[26] H. Kim, K. Dooley, E. Johnson, and S. W. North, Rev. Sci. Instrum. **76**, 124101 (2005).
[27] S. Arepalli, N. Presser, D. Robie, and R. J. Gordon, Chem. Phys. Lett. **117**, 64 (1985).
[28] D. J. Bamford, L. E. Jusinsk, and W. K. Bischel, Phys. Rev. A **34**, 185 (1986).
[29] A. T. Eppink and D. H. Parker, Rev. Sci. Instrum. **68**, 3447 (1997).
[30] B.-Y. Chang, R. C. Hoetzlein, J. A. Mueller, J. D. Geisler, and P. L. Houston, Rev. Sci. Instrum. **69**, 1665 (1998).
[31] V. Drinbinski, A. Ossadtchi, V. A. Mandelshtam, and H. Reisler, Rev. Sci. Instrum. **73**, 2634 (2002).
[32] H. M. Lambert, A. A. Dixit, E. W. Davis, and P. L. Houston, J. Chem. Phys. **121**, 10437 (2004).
[33] R. A. Durie and D. A. Ramsay, Can. J. Phys. **36**, 35 (1958).
[34] J. A. Coxon and D. A. Ramsay, Can. J. Phys. **54**, 1034 (1976).
[35] P. W. McLoughlin, C. R. Park, and J. R. Wiesenfeld, J. Mol. Spectrosc. **162**, 307 (1993).
[36] M. Trolier, R. L. Mauldin III, and A. R. Ravishankara, J. Phys. Chem. **94**, 4896 (1990).
[37] W. H. Howie, I. C. Lane, S. M. Newman, D. A. Johnson, and A. J. Orr-Ewing, Phys. Chem. Chem. Phys. **1**, 3079 (1999).
[38] The situation for the $A\ ^2\Pi_{3/2}-X\ ^2\Pi_{3/2}$ transition in ClO is, in fact, a bit more complicated than (6), where we have not taken into account that the wave functions for the initial and dissociative states are linear combinations of those for $\Omega=\pm(3/2)$. However, for strict case (a) behavior, it can be shown that the final formula using the correct linear combinations reduces to (6). See also the Appendix.
[39] U. Fano, Phys. Rev. **124**, 1866 (1961).
[40] J. B. Tatum and J. K. T. Watson, Can. J. Phys. **49**, 2693 (1971).
[41] B. R. Lewis, S. T. Gibson, M. Emami, and J. H. Carver, J. Quant. Spectrosc. Radiat. Transf. **40**, 1 (1988).
[42] P. C. Cross, R. M. Hainer, and G. W. King, J. Chem. Phys. **12**, 210 (1944).
[43] A computer program that calculates β and absorption intensity as a function of wave number and broadening parameters is available. It handles many common diatomic excitation cases as well as intermediate case (a) and case (b) behaviors. The program and examples are available at http://people.ccmr.cornell.edu/~plh2/group/Betaofnu.htm